Dynamics of "leaking" Hamiltonian systems

Judit Schneider,[1] Tamás Tél,[2] and Zoltán Neufeld[3]
[1]*Department of Physics, University of Potsdam, PF 601553, 14415 Potsdam, Germany*
[2]*Institute for Theoretical Physics, Eötvös University, Pf. 32, H-1538, Budapest, Hungary*
[3]*Department of Applied Mathematics and Theoretical Physics, University of Cambridge, Silver Street, Cambridge CB3 9EW, United Kingdom*
(Received 30 April 2002; published 30 December 2002)

In order to understand the dynamics in more detail, in particular for visualizing the space-filling unstable foliation of closed chaotic Hamiltonian systems, we propose to leak them up. The cutting out of a finite region of their phase space, the leak, through which escape is possible, leads to transient chaotic behavior of nearly all the trajectories. The never-escaping points belong to a chaotic saddle whose fractal unstable manifold can easily be determined numerically. It is an approximant of the full Hamiltonian foliation, the better the smaller the leak is. The escape rate depends sensitively on the orientation of the leak even if its area is fixed. The applications for chaotic advection, for chemical reactions superimposed on hydrodynamical flows, and in other branches of physics are discussed.

DOI: 10.1103/PhysRevE.66.066218 PACS number(s): 05.45.Ac

I. INTRODUCTION

Opening up closed chaotic Hamiltonian systems by a leak, i.e., by defining a finite region in their phase space through which escape is possible, leads to the escape of nearly all the trajectories, and to transiently chaotic behavior. We emphasize that this behavior is always related to the presence of a chaotic saddle which governs the motion of the long-lasting transients. The chaotic saddle, made visible by the leaking, is necessarily a subset of the original invariant space-filling set and can thus be considered as a skeleton of it.

The possibility of leaking a billiard to generate chaos with a finite lifetime was already mentioned in the classical paper by Pianigiani and Yorke on transient chaos [1]. Later this problem was discussed in detail in the context of fractal exit boundaries [2], of geometrical acoustics [3], as well as in the context of ergodicity [4] with fixed holes of exit. Another, more recent, reason for studying the motion in leaked systems is the Ott-Grebogi-Yorke (OGY) method of controlling chaos [5], in which a control region is defined inside of which the dynamics is changed to achieve control [6]. Furthermore, leaking can be relevant in many problems of celestial mechanics and cosmology, where gravitating bodies are considered to be point masses: by taking into account their finite sizes, the probability of collisions becomes nonzero. The simplest way of discussing this effect is to take out particles from the process after having hit other ones. This corresponds to leaking the phase space around the center of large bodies with arbitrary momenta [15]. A leaking method has also been applied to analyzing the chaotic structure of the mixmaster cosmological model [16]. A problem of great technological relevance is the design of heterostructure devices: in the ballistic regime, these nanoscale structures are—from the point of view of the electron's motion—billiards, leaked at the positions of the leads [17]. Characteristics of the transiently chaotic classical motion in these open billiards (such as, e.g., the escape rate) are known to be related to the statistics of the measured conductance fluctuations. In these investigations, the size of the leak is typically small and its position is unchanged.

Our aim here is to study whether the characteristics of transient chaos changes by changing the orientation of a large leak. In the chaotic region of closed Hamiltonian systems where the natural measure is uniform, one might expect that the escape process depends on the area of the leaked region only. Instead, we find that there is an essential dependence on the orientation even if the area is fixed. This dependence can be considered as a fingerprint of the unstable foliation of the chaotic region, which is not visible as a phase-space structure in the closed case but becomes observable by the smallest amount of leaking. We point out that the anisotropy of this foliation (together with the finite size of the leak) is responsible for the observed orientation dependence.

One motivation for considering finite leaks comes from hydrodynamics, from the so-called resetting algorithm for studying chaotic stirring in fluids as proposed by Pierrehumbert [7]. Here one studies passive advection by two-dimensional incompressible closed flows, which leads to a particle dynamics with a closed Hamiltonian phase space. Resetting is realized by selecting two finite regions of the flow. In any of them, a certain color is given the particle that will be carried until entering the other region where the color is changed again. This algorithm can be considered to be an elementary model of chemical reactions, since the fluid parcels can have certain properties that they will lose by reaching one of the preselected regions. After returning from there, they therefore behave differently from the point of view of chemical activity, which is marked by the change of their colors. This simple algorithm is sufficient to make clear filamentational patterns visible in the flow.

A recent discovery [8] in the field of realistic chemical reactions superimposed on closed flows shows that the product distribution can be filamental in spite of the fact that the passive problem has a Hamiltonian chaotic dynamics. The chemistry is visualizing in this case the unstable filamentation. We claim that the leaking of the passive problem makes

the same filamentation visible as the routes of particles that are about to escape. The plots exhibiting the unstable manifolds of the leaked system, therefore, show striking similarities to those of the product distribution in unleaked flows with reactions.

The paper is organized as follows. In the next section, we summarize our numerical findings for three model systems: the area-preserving baker map, the so-called sine map, and its random version. In all cases the dependence of the chaotic saddle is investigated on the size and orientation of the leak.

II. NUMERICAL PROCEDURE AND RESULTS

In contrast to previous studies, we investigate the effect of large leaks and take a band crossing through the full phase space as the leak. Its center is chosen to be the center of the phase space. One freely changeable parameter is then the width ε of the band in the x direction (which also measures the area) and the angle θ of its axis relative to a fixed direction.

The analysis is carried out in the spirit of the theory of transient chaos [9]: the basic aim is to identify the set of never-escaping orbits, a nonescaping chaotic set, the so-called chaotic saddle, along with its stable and unstable manifolds. The characteristic number to be measured is the escape rate κ versus ε and θ. The invariant sets are determined by means of the method described in [10]. We start with a large number N_0 of particles initially distributed in the full phase space uniformly. All the nonescaping particles are followed over a large number of iterations, say n. For large enough N_0 and n, the initial coordinates of the nonescaping particles should trace out the stable manifold, their final positions after n steps of the unstable manifold, and the midpoints at time $n/2$ of the chaotic saddle itself. The reason for this is that [from regions outside of eventually existing Kolmogorov-Arnold-Moser (KAM) tori] all initial points exit with the exception of a fractal set of measure zero. Therefore, points spending a long time in the leaked system must be those that came close to the chaotic set. The points still inside after n steps are thus either on the chaotic saddle or are already about to leave it. If so, they are practically on the unstable manifold. A long time ($n/2$ steps) earlier they must have been around the saddle, and initially around the stable manifold.

The basic quantity we use to measure the degree of openness is the escape rate κ from the chaotic saddle. The number of $N_n - N_\infty$ of surviving points after n steps (N_∞ stands for the never-escaping points due to the presence of KAM tori) should decrease after a large number of steps as $\exp(-\kappa n)$. The escape rate was determined by measuring the number $N_n - N_\infty$ of survivors and fitting a straight line to the $\ln(N_n - N_\infty)$ versus n curve.

A. The baker map

As a very simple example in which no KAM tori can be present, we take the area-preserving baker map [11]. The dynamics is defined on the unit square. The lower half square is compressed along the x axis to its half and is stretched along the y axis by a factor of 2 so that the left lower corner, the origin, is kept fixed. The upper half square is transformed in a similar way but the upper right corner, the point (1, 1), is left unchanged during this process. The system is known to be fully hyperbolic, all local Lyapunov exponents are $\ln 2$, and therefore no stability islands are present. The natural distribution is uniform on the full square.

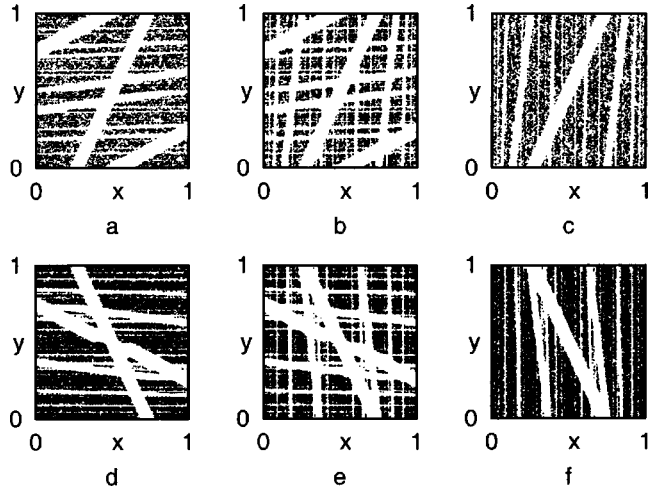

FIG. 1. The stable manifold, the chaotic saddle, and the unstable manifold of the leaked baker map with $\varepsilon = 0.1$ in the case of a tilted leak with angle $\theta = 25°$ [(a)–(c)] and $\theta = -25°$ [(d)–(f)]. The parameters of the simulations are $N_0 = 10^6$ and $n = 40$. The different contrast of the pictures is due to the different decays: the number of remaining particles is $N_{40} = 9537$ ($N_{40} = 22\,399$) in the 25° ($-25°$) case so that the escape rate is $\kappa(25°) = 0.11$ [$\kappa(-25°) = 0.09$].

Figure 1 shows the saddle and its manifolds in the case of a leak with a width and area of $\varepsilon = 0.1$ and located at angles $\theta = \pm 25°$ relative to the vertical line going through the midpoint of the unit square. The leak is clearly visible as a white band. There are many more white bands present: in the plot of the stable (unstable) manifold, these are the preimages (images) of the leak, and in the plot of the saddle both the preimages and the images are present. Although the baker map is thought to be symmetric around the midpoint of the square, its action on full lines crossing the unit square is not. This is quite clear in the first images of the leak [bands of second largest width in Figs. 1(c) and 1(f)], but the effect is even stronger in the case of the first preimages [bands of second largest width in Figs. 1(a) and 1(d)]. The preimages of left- and right-tilted bands are completely different. The inverse map transforms the left (right) half square on the lower (upper) half square. Therefore, the lower part of the 25° leak is mapped on a band around the lower right corner, while that of the $-25°$ leak is mapped on a band around the lower left corner of the second quadrant, etc. More importantly, the first preimage of the 25° leak does not overlap with the leak, but there is an overlap in the other case. Thus, the total area of the leak and its first preimage is larger for the positive angle case than for the negative one. This asymmetry is kept by further iterations leading to different values of the escape rate: $\kappa(25°) > \kappa(-25°)$. The difference in the escape rate can be deducted from the darkness of the invariant sets, too, since we used the same number of initial

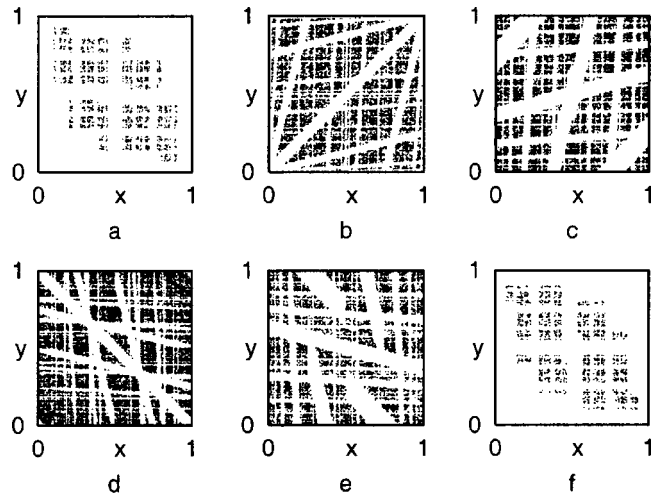

FIG. 2. The chaotic saddles of the leaked baker ($\varepsilon=0.1$) at leak angles $\theta=0°$ (a), 45° (b), and 75° (c), and $\theta=-45°$ (d), $-75°$ (e), and $\mp 90°$ (f). The parameters of the simulations are $N_0=10^6$ and $n=40$. In order to ensure that the leak area is always ε, at leak angles $\theta=\pm 45°$ [(b) and (d)] we added tiny leak pieces around the corners not crossed by the main band, as if the map were periodic. Contrast differences can be observed again.

conditions and therefore more points (smaller escape rate) imply darker figures.

Figure 2 is an overview of the chaotic saddles for the same width but at other angles θ. The completely different textures at angles of opposite signs are striking.

The dependence of the escape rate on both parameters is summarized in Fig. 3. The escape rate belonging to very narrow leaks is nearly orientation-independent. In addition, the value of κ is then close to the total relative area of the leak, which is ε in our case. Orientation dependence becomes considerable by $\varepsilon=0.1$, and the amount of fluctuations around the mean is increasing with increasing area. In all cases, the naive expectation $\kappa=-\ln(1-\varepsilon)$ is close to or below the average escape rate over all the angles.

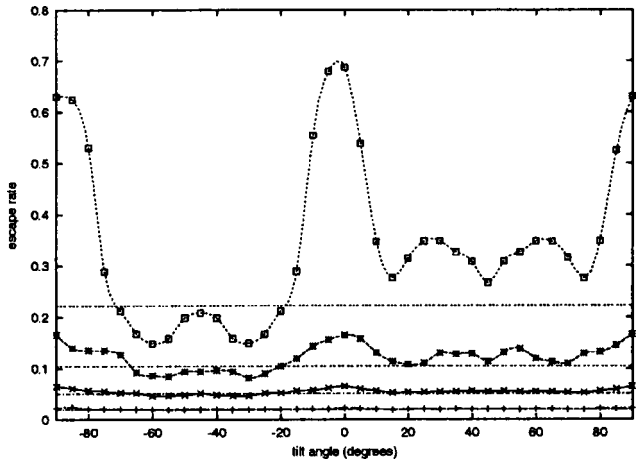

FIG. 3. The dependence of the escape rate on the tilt angle at different widths $\varepsilon=0.02$ (+), 0.05 (x), 0.1 (*), and 0.2 (squares). Horizontal lines correspond to the values $\kappa=-\ln(1-\varepsilon)$.

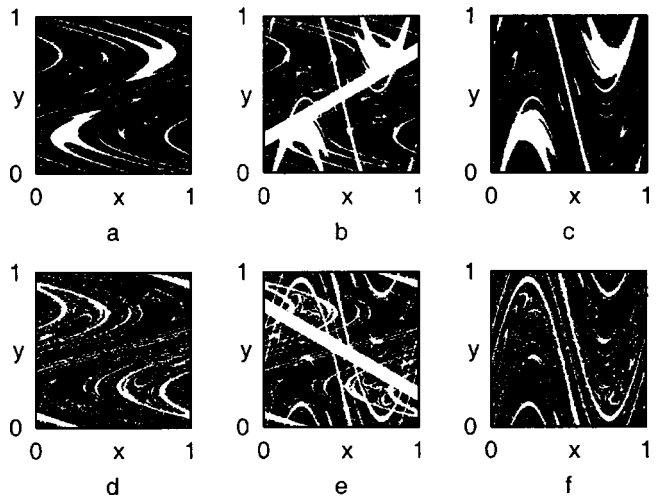

FIG. 4. The stable manifold, the chaotic saddle, and the unstable manifold of the leaked sine map with $\varepsilon=0.1$ in the case of a tilted leak under angle $\theta=60°$ [(a)–(c)] and $\theta=-60°$ [(d)–(f)]. Because the particles are distributed over the full square initially, all plots contain the KAM tori as very dark structures. In order to emphasize more strongly the stable and unstable foliation, in parts (a), (c), (d), and (f) we do not show the leak. The leak is, however, clearly visible in the plots of the chaotic saddles [(b) and (e)] as the widest white band. The parameters of the simulations are $N_0=10^5$ and $n=20$.

B. The sine map

Next we consider the sine map introduced in [7]. It is a double periodic map defined on the unit square whose action is the subsequent application of two sinusoidal displacements, one in the x, the other one in the y direction. The explicit form of the map is

$$x_{n+1}=x_n+a\sin(2\pi y_n+\phi_n) \mod 1,$$
$$y_{n+1}=y_n+a\sin(2\pi x_{n+1}+\phi_n) \mod 1. \tag{1}$$

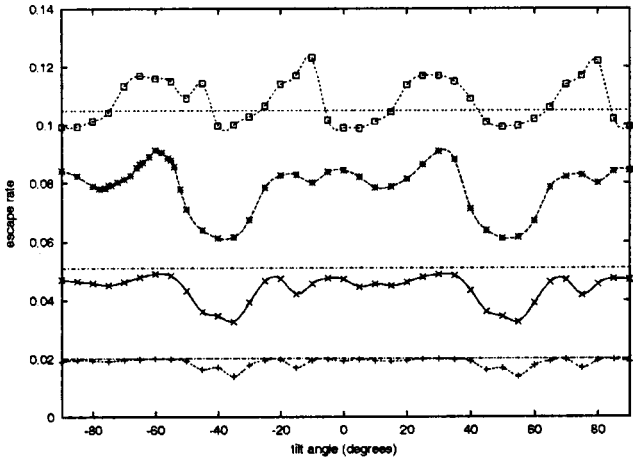

FIG. 5. The dependence of the escape rate on the tilt angle at different widths $\varepsilon=0.02$ (+), 0.05 (x), 0.1 (*), and 0.2 (squares). Horizontal lines correspond to the values $\kappa=-\ln(1-\varepsilon)$. The one belonging to $\varepsilon=0.2$ is beyond the frame.

We will use the amplitude $a=0.6$.

First, all the phase variables will be taken to be zero: $\phi_n \equiv 0$. In this case, the map represents a typical, closed Hamiltonian system [7,12] containing islands of integrability and broken KAM tori (cantori).

These regions are clearly visible in the invariant sets (Fig. 4) since due to the homogeneous initial distribution, points starting in these regions escape very slowly or do not escape at all, hence the very dark structures appearing in the plots. Again, the asymmetry due to the leak orientation is clear.

In the escape rate versus ε and θ diagram of Fig. 5, we see again that leaks with small area have the weakest orientation dependence. The escape rate is then well approximated by the area ε of the leak. At larger areas, however, fluctuations become stronger. It can be seen from Fig. 5 that leak angles coinciding with the slope of the local unstable and stable foliation ($\theta=-20°$ and 70° in the sine map, and 0° and $\pm 90°$ in the baker map) always belong to a local maximum of the escape rate (which is a global one in the baker map). No simple rules have been found for predicting the angles of the other local maxima. In this case, the $\kappa(\theta)$ diagram exhibits an invariance under translations with 90°.

The naive expectation $\kappa=-\ln(1-\varepsilon)$ is now *above* the average escape rate over the angles. In the case of the largest area investigated, it is much larger than any of the measured escape rates. We attribute this to the presence of the KAM tori and cantori, and to their remnants after leaking. These surfaces are known to be sticky and the long-time decay from their neighborhood is not even exponential, but of power-law type [13]. We are interested in the intermediate time behavior, which is found to be still exponential, but the presence of these surfaces also makes the effective escape rate κ smaller than in cases without tori. This is why the naive expectation now becomes an upper bound. In fact, an even larger upper bound follows if the total surface of all the KAM regions is added to ε.

Consider now what happens in the case of a gradual decrease of the width of ε (at fixed angle). The chaotic saddle and its manifolds become denser and denser. In the limit $\varepsilon \to 0$, the escape rate disappears, the chaotic saddle becomes the full chaotic sea, and the stable and unstable manifolds trace out the (area-filling) stable and unstable foliation of the chaotic sea. The leaked system's manifolds thus provide an approximant to the closed Hamiltonian foliation, the better the smaller the leak is. The leaked system's (un)stable manifold is a piece of the closed system's (un)stable foliation. Furthermore, in a numerical approach, the manifolds fill in the full square at a finite value of ε already, due to the finite width of the lines of the plot. Therefore, for a visually well observable representation of the closed Hamiltonian foliation, a small but finite value of ε is needed. Thus, for example, Figs. 4(d) and 4(f) can be considered as a good approximant of the closed foliation [while Figs. 4(a) and 4(c) less accurate ones].

These qualitative findings are valid for any shape and location of the leak. We carried out numerical experiments also with two-band leaks under various angles and at different locations.

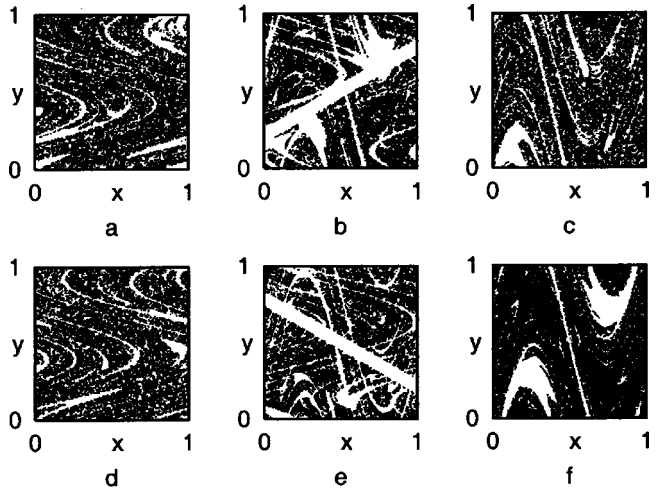

FIG. 6. The same as Fig. 4 for the random sine map. The topological structure is similar but the difference in contrast is greatly diminished.

C. The random sine map

The random version of the sine map is obtained by considering random phases, i.e., by taking the values ϕ_n of Eq. (1) at any instant of discrete time n from a stationary ensemble from the range $(-\pi,\pi)$. The map remains area-preserving with these phases, too, but the presence of the random perturbation leads to the disappearance of any invariant tori [7,14]. This might, however, be observed in numerical simulations on long time scales only. In the fluid-dynamical context, the random version of the map represents the advection problem in an incompressible (smooth, nonturbulent) flow with an aperiodic (chaotic) time dependence. The basic difference relative to the previous cases is that the chaotic saddle and the manifolds are no longer independent of the number n of iterations taken, not even for large values of n. Their shapes are changing with n (since the random phases do so) but their fractal dimensions do not. Therefore, the plots look qualitatively similar irrespective of the value of n used.

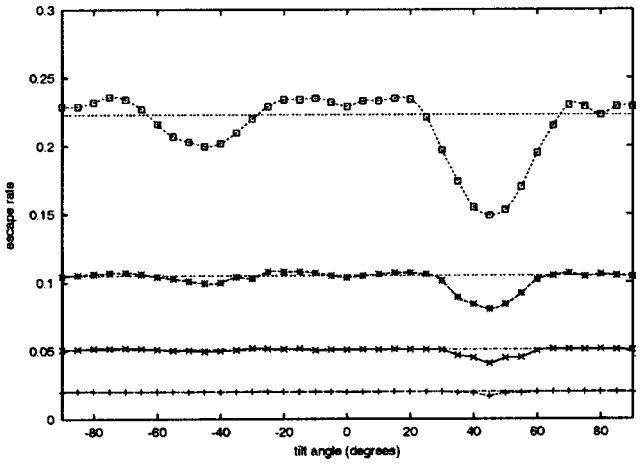

FIG. 7. The dependence of the escape rate on the tilt angle at different widths $\varepsilon=0.02$ (+), 0.05 (x), 0.1 (*), and 0.2 (squares) for the random sine map. Horizontal lines correspond to the values $\kappa=-\ln(1-\varepsilon)$.

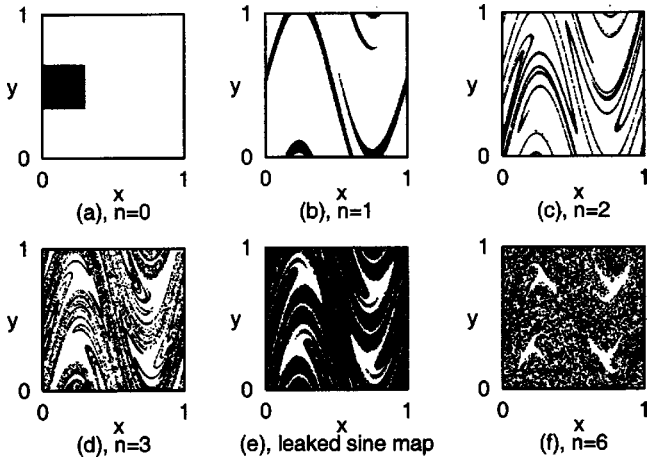

FIG. 8. The shape of a square droplet ($N_0=10^4$) at time $n=0$ (a), $n=1$ (b), $n=2$ (c), $n=3$ (d), and $n=6$ (f) in the nonrandom sine map. Part (e) is the unstable manifold of the chaotic saddle ($N_0=7\times10^5$) obtained by leaking the map with two identical bands parallel to the y axis of width $\varepsilon=0.1$ and midpoints at (0.25,0.5) and (0.75,0.5).

Figure 6 shows the invariant sets. The former dark spots are no longer present because of the disappearance of coherent phase-space structures.

Considering the dependence of the escape rate on the orientation, we find (Fig. 7) that the fluctuations are reduced. This can be interpreted by observing that the random phases indicate a shift of the filamentation in a certain direction. Since the leak is fixed, the filamentation under it is time-dependent, and hence an averaging procedure is carried out. This leads to a much weaker orientation dependence than in the nonrandom case.

In addition, the value of the escape rate comes closer to the naive expectation $\kappa=-\ln(1-\varepsilon)$ since sticky phase-space surfaces are efficiently destroyed by the randomness of the phase.

Note that there are two minima of the κ versus tilt angle curve shown in Fig. 7 obtained from simulations carried out over 20 time steps. By following ensembles of particles over longer times and deducing κ as the asymptotic decay rate, we observe that the minimum values become closer to each other, and to the naive expectation as well; the curve becomes better smoothed out. It is worth mentioning that by randomly choosing the position of the center of the leak along the x or y axis (at fixed tilt angle) and by using the nonrandom sine map, the orientation dependence of the escape rate fully vanishes and this can already be seen over short time scales.

III. CONCLUSIONS

From the point of view of the application of the resetting algorithm [7] described in the Introduction, our results imply that the patterns depend not only on the size of the resetting region but on its orientation, too. This dependence disappears, however, if the flow is sufficiently random, or sufficiently chaotic.

Another implication of our findings can be a proper interpretation of transient droplet patterns in closed flows. The initial droplet is compact; its dimension is 2. As time goes on, the droplet is stretched and folded (its area is unchanged) and becomes elongated along the unstable filamentation of the flow. There might be an instant of time at which the shape of the droplet is similar to the unstable manifold of the leaked flow with a certain width and orientation of the leak [Fig. 8(d) is quite similar to Fig. 8(e)]. This does not mean, however, that the droplet's shape is the same on *all* scales as the unstable manifold. It does not have, in any instant, a well-defined fractal dimension [13]. In fact, its form appears to be denser already after three more steps [Fig. 8(f)]. The only stage where its dimension is well defined [13] is that of the asymptotic state reached after an infinitely long time, when it fills the full chaotic region (and its dimension is 2 again).

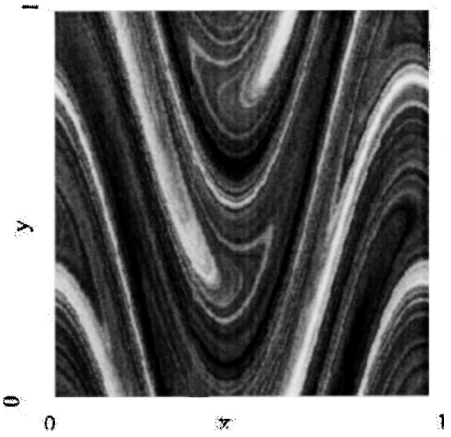

FIG. 9. Chemical concentration field of problem (2) obtained by iterating the sine map with random phases at $a=0.7$. Bright areas indicate regions of high concentration.

In a general hydrodynamical problem, it is natural to find regions of qualitatively different flow features (such as, e.g., jets, recirculating regions, eddies, etc.). One can then select one of these regions and consider all others as leaks in order to determine the escape rate, which is a measure of material exchange of this region with its surroundings. Small values of the escape rate mark regions with large lifetimes of water which might therefore be of specific biological relevance.

The next property we discuss is the relation to filamental chemical or biological product distributions in closed flows. We have considered a very simple chemical reaction, the decay of the concentration C of some chemical constituent towards a background value superimposed on the random sine map as a hydrodynamical flow. The chemical field $C(x,y)$ is generated by the mapping

$$C_{n+1}=S(x_n,y_n)+bC_n,$$

$$x_{n+1}=[x_n+a\sin(2\pi y_n+\phi_n)] \mod 1,$$

$$y_{n+1}=[y_n+a\sin(2\pi x_{n+1}+\phi_n)] \mod 1, \qquad (2)$$

where $S=S_0+S_1\sin(2\pi x)\sin(2\pi y)$ is a fixed source distribution and the parameter b ($b<1$) is a measure of the decay rate. In each step, the chemical concentration decays by a

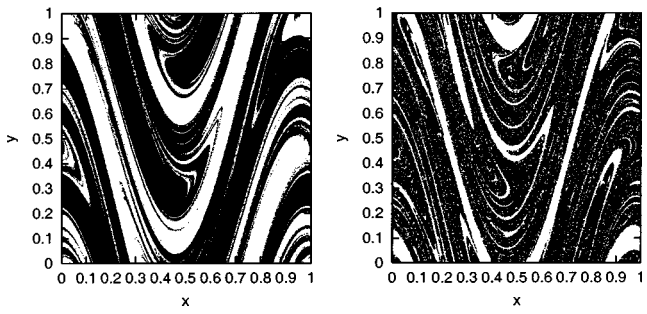

FIG. 10. Left picture: The concentration distribution of problem (2) in the random sine map after 10 steps of iteration starting from an initially homogeneous distribution. Black regions correspond to concentrations higher than the threshold value $C_{\mathrm{th}}=1$. Right picture: The unstable manifold of the chaotic saddle in the leaked passive problem obtained by using the same random sequence. The width of the leak is taken as 0.1.

factor b (in our case $b=0.5$) and receives an input $S(x,y)$ according to the local source concentration. Then the fluid parcels are advected by the random sine map ($a=0.7$). Figure 9 shows the concentration distribution obtained in this way. It has a striking filamental structure since the parameter values correspond to a state beyond the smooth-filamental transition defined and described in [8]. Because the concentration is smooth along the unstable direction only, directions corresponding to low gradients trace out a part of the unstable foliation. In the left picture of Fig. 10, only the regions of high concentration ($C>1$) are plotted. The boundary between black and white regions, corresponding to an isoconcentration surface, shows a subset of the unstable foliation. It is therefore not surprising that the unstable manifolds of the leaked passive system, which is also a subset of the unstable foliation [right picture of Fig. 10(b)], trace out a similar structure.

Leaking the underlying Hamiltonian system provides a computationally cheap and efficient method for visualizing the unstable foliation, by which one can reconstruct structures traced out by active processes, for example structures related to phytoplankton distributions in the Gulf Stream [8,18].

In conclusion, the geometric structure of the unstable foliation of a closed Hamiltonian problem is the origin of the strong dependence of the escape rate on the orientation of the leak. Local maxima of this function correspond to the direction of the unstable or the stable foliation. The randomness of the dynamics is smoothening out the orientation dependence. The method can also be used to indicate the presence of KAM islands since the effective escape rate in nonrandom cases is then smaller than the naive expectation. Measuring the escape rate of leaked area-preserving systems can give a useful piece of information about the unstable foliation of the closed system, whose fingerprints otherwise only appear as instantaneous droplet shapes.

Our findings might have relevance beyond the field of hydrodynamics, in all the examples mentioned in the Introduction (billiard, acoustic, control, celestial mechanics, etc.). In particular, for mesoscopic devices in the ballistic regime, we predict a strong dependence of the escape rate and hence of conductance fluctuations on the actual position of the leads (at fixed width) along the wall of the billiard.

ACKNOWLEDGMENTS

Useful discussions are acknowledged with H. Buljan, R. Dorfman, P. Grassberger, C. Grebogi, H. Kantz and K. G. Szabó. This research has been supported by the Hungarian Research Foundation (OTKA T032423). J.S. is thankful for financial support from the DAAD, the Max Planck Research School for Biomimetic Systems (IMPRS), and the Society Freunde der TU. T.T. is thankful to Professor E. Schöll for kind hospitality. J.S. and T.T. were supported by the DAAD 324/PPP-Ungarn-ssch.

[1] G. Pianigiani and J. A. Yorke, Trans. Am. Math. Soc. **252**, 351 (1979).
[2] S. Bleher, C. Grebogi, E. Ott, and R. Brown, Phys. Rev. A **38**, 930 (1988).
[3] O. Legrand and D. Sornette, Europhys. Lett. **11**, 538 (1990).
[4] A. Lopes and R. Markarian, SIAM (Soc. Ind. Appl. Math.) J. Appl. Math. **56**, 651 (1996); N. Chernov and R. Markarian, Bol. Soc. Bras. Math **28**, 271 (1997); N. Chernov, R. Markarian, and Troubetzkoy, Ergod. Theory Dyn. Syst. **18**, 1049 (1998); **20**, 1007 (2000).
[5] E. Ott, C. Grebogi, and J. A. Yorke, Phys. Rev. Lett. **64**, 1196 (1990).
[6] V. Paar and N. Pavin, Phys. Rev. E **55**, 4112 (1997); V. Paar and H. Buljan, *ibid.* **62**, 4869 (2000); H. Buljan and V. Paar, *ibid.* **63**, 066205 (2001).
[7] R. Pierrehumbert, Chaos, Solitons Fractals **4**, 1091 (1994).
[8] Z. Neufeld, C. López, and P. Haynes, Phys. Rev. Lett. **82**, 2606 (1999); Z. Neufeld *et al.*, Phys. Rev. E **61**, 3857 (2001); C. López *et al.*, Phys. Chem. Earth **26**, 313 (2001).
[9] T. Tél, in *Directions in Chaos*, edited by Hao-Bai Lin (World Scientific, Singapore, 1990), p. 149.
[10] Y.-C. Lai, T. Tél, and C. Grebogi, Phys. Rev. E **48**, 709 (1993).
[11] E. Ott, *Chaos in Dynamical Systems* (Cambridge University Press, Cambridge, England, 1993).
[12] Z. Neufeld, P. Haynes, and G. Picard, Phys. Fluids **12**, 2506 (2000).
[13] F. Christiansen and P. Grassberger, Phys. Lett. A **181**, 47 (1993); Y. Lau, J. Finn, and E. Ott, Phys. Rev. Lett. **66**, 978 (1991).
[14] J. Jacobs, E. Ott, T. Antonsen, and J. Yorke, Physica D **110**, 1 (1997); Z. Neufeld and T. Tél, Phys. Rev. E **57**, 2832 (1998).
[15] J. Nagler (private communications).
[16] A. E. Motter and P. S. Letelier, Phys. Lett. A **285**, 127 (2001).
[17] M. L. Roukes and O. L. Alerhand, Phys. Rev. Lett. **65**, 1651 (1990); S. Ree and L. E. Reichl, Phys. Rev. E **65**, 055205 (2002); H.-S. Sim and H. Schomerus, e-print cond-mat/0203091.
[18] J. Schneider and T. Tél (unpublished).